Supplementary Material

Feedforward Compensation of Piezo Nonlinearity for High-Precision High-Speed Atomic Force Microscopy

Kenichi Umeda[1,2] and Noriyuki Kodera[1]

[1] *Nano Life Science Institute (WPI-NanoLSI),*

Kanazawa University, Kakuma-machi, Kanazawa, Ishikawa, 920-1192, Japan.

[2] *PRESTO/JST, 4-1-8 Honcho, Kawaguchi, Saitama 332-0012, Japan.*

Table S1. Nomenclature list of variables

Symbol	Description
V_{Max}	Maximum output voltage of the piezo driver
V_{offset}	Scan center position (X/Y offset voltage)
p_{offset}	V_{offset} normalized by V_{Max}
m_{offset}	Correction factor for V_{offset} dependence
$m_{\mathrm{offset}-}$ and $m_{\mathrm{offset}+}$	m_{offset} at $p_{\mathrm{offset}} = -1$ and $p_{\mathrm{offset}} = +1$
α_{offset} and β_{offset}	Linear and quadratic coefficients for V_{offset} nonlinearity correction
R_{scan}	Scan range
$R_{\mathrm{scan,x}}$	Scan size in the X direction
V_{scan}	Amplitude of the scan signal
$\tilde{V}_{\mathrm{scan}}$	V_{scan} normalized by V_{Max}
R_{base}	Base scan size used as a reference for calibration for R_{scan} nonlinearity correction
k_{scan}	Piezoelectric coefficient obtained by linear approximation
α_{scan} and β_{scan}	Scaling and nonlinear factors of the piezoelectric coefficient for R_{scan} nonlinearity correction
$\tilde{V}_{\mathrm{th}}$	Normalized threshold voltage for switching between the quadratic ($\tilde{V}_{\mathrm{scan}} \leq \tilde{V}_{\mathrm{th}}$) and linear extrapolation ($\tilde{V}_{\mathrm{scan}} > \tilde{V}_{\mathrm{th}}$) expressions for R_{scan} nonlinearity correction
R_{th}	Threshold R_{scan} corresponding to $\tilde{V}_{\mathrm{th}}$
V	Time-dependent scan signal
t	Time normalized by the line-scan period
i (subscript)	$i = 1$ and $i = 2$ denote the forward and backward scans, respectively
τ_i	Normalized ideal linear waveform
α_{turn}	Turning point between forward and backward scans
$\alpha_{\mathrm{turn,x}}$	α_{turn} for X scan
$\alpha_{\mathrm{turn,y}}$	α_{turn} for Y scan
G_{piezo}	Piezo nonlinear transfer function
β_i	Nonlinear factors of the scan waveforms

$\beta_i^{\max}$	Maximum β_i at $V_{\text{scan}} = V_{\text{Max}}$
u_i	Normalized nonlinear waveform
$u_{\text{peak},i}$	u_i at which the hysteresis is maximized
$u_{\text{peak},i}^{(0)}$	$u_{\text{peak},i}$ in the limit as $\beta_i \to 0$
λ_i	Linear term for harmonic model
ξ_i,	Nonlinearity parameter for harmonic model
γ_i	Asymmetry parameter for harmonic model
ρ_i	Exponential coefficient in the correlation equation between β_i and V_{scan}
m_{freq}	Correction factor for frequency dependence
f_{scan}	Scan frequency
f_{ref}	Reference scan frequency used during calibration
f_{fps}	Frame rate
$f_{\text{c,DH}}$	Cutoff frequency of dynamic hysteresis
α_{DH}	Logarithmic slope associated with dynamic hysteresis
$N_{\text{y,total}}$	Total number of Y pixels in the forward and backward scans
$N_{\text{y,fwd}}$	Number of Y pixels in the forward scan
v_{scan}	Scan velocity

Supplementary Note 1: Fourier transform of nonlinear models

In the main text, we analyzed piezo nonlinearity compensation by comparing the sinusoidal model with the harmonic model. In practice, the Fourier-series representations are used instead of the time-domain functions to suppress high-frequency components and avoid exciting piezo resonances. In this note, the corresponding expansions are given below. For the harmonic model, Eq. (18) is expanded as a Fourier series as follows:

$$f(t) = a_0 + 2\sum_{n=1}^{\infty}\left[a_n \cos(n\omega t) + b_n \sin(n\omega t)\right], \tag{S1}$$

with the Fourier coefficients given by

$$\begin{aligned} a_0 = {} & \alpha_{\text{turn}}\left[\beta_1\left(\frac{2}{\pi}-\gamma_1\right)+\frac{\lambda_1}{2}\right] \\ & -(1-\alpha_{\text{turn}})\left[\beta_2\left(\frac{2}{\pi}-\gamma_2\right)+\frac{\lambda_2}{2}-1\right], \end{aligned} \tag{S2}$$

$$\begin{aligned} a_n = {} & \frac{1}{p_n}\left[\begin{array}{l}\lambda_1\left(\dfrac{\cos q_n - 1}{q_n}+\sin q_n\right) \\ +\lambda_2\dfrac{\cos q_n - 1}{p_n - q_n} - \sin q_n\end{array}\right], \\ & -\frac{\beta_1}{4\alpha_{\text{turn}}^2 n^2 - 1}\left[\frac{\alpha_{\text{turn}}(\cos q_n + 1)}{\pi} + \gamma_1\frac{(8\alpha_{\text{turn}}^2 n^2 - 1)\sin q_n}{p_n}\right] \\ & +\frac{\beta_2}{4(1-\alpha_{\text{turn}})^2 n^2 - 1}\left[\frac{(1-\alpha_{\text{turn}})(\cos q_n + 1)}{\pi} + \gamma_2\frac{\sin q_n}{p_n}\right], \end{aligned} \tag{S3}$$

$$\begin{aligned} b_n = {} & \frac{1}{p_n}\left[\begin{array}{l}\lambda_1\left(\dfrac{\sin q_n}{q_n}-\cos q_n\right) \\ +\lambda_2\left(\dfrac{\sin q_n}{p_n - q_n}+1\right)+\cos q_n - 1\end{array}\right] \\ & -\frac{\beta_1}{4\alpha_{\text{turn}}^2 n^2 - 1}\left[\frac{\alpha_{\text{turn}}\sin q_n}{\pi} - \gamma_1\frac{(8\alpha_{\text{turn}}^2 n^2 - 1)\cos q_n + 1}{p_n}\right] \\ & +\frac{\beta_2}{4(1-\alpha_{\text{turn}})^2 n^2 - 1}\left[\frac{(1-\alpha_{\text{turn}})\sin q_n}{\pi} + \gamma_2\frac{1-8(1-\alpha_{\text{turn}})^2 n^2 - \cos q_n}{p_n}\right], \end{aligned} \tag{S4}$$

where

$$p_n = 2\pi n, \tag{S5}$$

$$q_n = 2\pi\alpha_{\text{turn}} n. \tag{S6}$$

Note that the Fourier coefficients become indeterminate when α_{turn} satisfies the conditions:

$$\alpha_{\text{turn}} = \frac{1}{2n} \text{ or } \alpha_{\text{turn}} = 1 - \frac{1}{2n}. \tag{S7}$$

To avoid this, α_{turn} should be slightly offset whenever either condition is met.

While the sinusoidal model (Eq. (16)) yields less complete compensation than the harmonic model, its simple form enables straightforward implementation. By substituting γ_i = 0, the Fourier coefficients of the sinusoidal model are obtained as follows:

$$a_0 = \frac{\alpha_{\text{turn}}\left(4\beta_1 + \pi\right) - \left(1 - \alpha_{\text{turn}}\right)\left(4\beta_2 - \pi\right)}{2\pi}, \tag{S8}$$

$$\begin{aligned} a_n = &\frac{\cos q_n - 1}{\left(1 - \alpha_{\text{turn}}\right)\alpha_{\text{turn}} p_n^2} \\ &+ K_n\left(1 + \cos q_n\right), \end{aligned} \tag{S9}$$

$$\begin{aligned} b_n = &\frac{\sin q_n}{\left(1 - \alpha_{\text{turn}}\right)\alpha_{\text{turn}} p_n^2} \\ &+ K_n \sin q_n, \end{aligned} \tag{S10}$$

where

$$K_n = \frac{1}{\pi}\begin{bmatrix} -\beta_1 \dfrac{\alpha_{\text{turn}}}{4\alpha_{\text{turn}}^2 n^2 - 1} \\ +\beta_2 \dfrac{1 - \alpha_{\text{turn}}}{4\left(1 - \alpha_{\text{turn}}\right)^2 n^2 - 1} \end{bmatrix}. \tag{S11}$$

By substituting $\beta_1 = \beta_2 = 0$, a more simple expression representing a linear sawtooth-like waveform is obtained, as follows:

$$a_0 = \frac{1}{2}, \tag{S12}$$

$$a_n = \frac{\cos q_n - 1}{\left(1 - \alpha_{\text{turn}}\right)\alpha_{\text{turn}} p_n^2}, \tag{S13}$$

$$b_n = \frac{\sin q_n}{\left(1-\alpha_{\text{turn}}\right)\alpha_{\text{turn}} p_n^2}. \tag{S14}$$

Supplementary Note 2: Analysis of sinusoidal model

To compensate for the piezo's nonlinear response, a function with the corresponding inverse transfer characteristic is required. To evaluate whether an assumed function is suitable for compensation, its agreement with the piezo's nonlinear response must be examined. In this note, we analyze the sinusoidal model given in Eq. (16). Although its inverse cannot be obtained explicitly, the peak residual and peak position can be derived analytically as described below.

Rearranging τ_i for the forward scan (i = 1) in Eq. (16) yields the following implicit equation:

$$\tau_1 = u - \beta_1 \sin\left(\pi\tau_1\right). \tag{S15}$$

To match the inverse transfer characteristic with the piezo response, it is important to analyze the residual relative to the linear component of the inverse transfer characteristic, which is derived as follows:

$$\Delta\tau_1 = \tau_1 - u \approx -\beta_1 \sin\left(\pi\tau_1\right). \tag{S16}$$

The peak position of the residual can be determined from the point where the slope of the function is zero,

$$\frac{\mathrm{d}\Delta\tau_1}{\mathrm{d}\tau_1} = -\pi\beta_1 \cos\left(\pi\tau_1\right) = 0, \tag{S17}$$

which gives

$$\tau_1\left(u = u_{\mathrm{peak},1}\right) = \frac{1}{2}. \tag{S18}$$

Substituting this expression into Eq. (S16) yields the residual peak as follows:

$$\Delta\tau_1(u = u_{\mathrm{peak},i}) = -\beta_1. \tag{S19}$$

Substituting Eqs. (S18) and (S19) into Eq. (S16) gives Eq. (17). The same expression is obtained for the backward scan (i = 2) by an analogous calculation.

Supplementary Note 3: Scaling error due to hysteresis

In this note, we examine the scaling error in AFM images arising from piezo hysteresis. As shown in Fig. 5(c), the piezo response closely resembles the sinusoidal model with the sign of the sine term reversed, and can be approximated by the following equation:

$$d(\tau_i) = \begin{cases} \tau_1 - \beta_1 \sin\left(\pi\tau_1\right) & \text{for } 0 < t \le \alpha_{\text{turn}}, \\ \tau_2 + \beta_2 \sin\left(\pi\tau_2\right) & \text{for } \alpha_{\text{turn}} < t \le 1, \end{cases} \tag{S20}$$

where d denotes the normalized nonlinear piezo response, varying from 0 to 1 in the forward scan and from 1 to 0 in the backward scan. β_1 and β_2 represent the nonlinear factors of the forward and backward scan waveforms, respectively.

Since the effective piezoelectric coefficient corresponds to the slope of the piezo response, it can be derived by differentiating Eq. (S20) as follows:

$$d'(\tau_1) = 1 - \pi\beta_1 \cos\left(\pi\tau_1\right) \quad \text{for } 0 < t \le \alpha_{\text{turn}}. \tag{S21}$$

The scaling error Δx is defined as the deviation from the ideal linear slope and is given by

$$\Delta x(t) = d'(t) - 1 = -\pi\beta_1 \cos\left(\pi\tau_1\right) \quad \text{for } 0 < t \le \alpha_{\text{turn}}. \tag{S22}$$

Therefore, Δx approaches zero near the image center, whereas the image is enlarged by up to a factor of $\pi\beta_i$ at the left edge ($\tau_1 = 0$) and reduced by up to the same factor at the right edge ($\tau_1 = 1$). This trend is reversed in the backward scan. Consequently, the maximum peak-to-peak scaling error over the entire image is approximately expressed as $2\pi\beta$ ($\approx 6\beta$).

In contrast, as shown in Fig. 5c, when the nonlinear compensation model produces overcompensation, a single node appears near the center of the image; the behavior can therefore be approximated by:

$$d(\tau_i) = \tau_1 - \beta_1 \cos\left(\pi\tau_1\right) \quad \text{for } 0 < t \le \alpha_{\text{turn}} \tag{S23}$$

Applying the same procedure to evaluate the scaling error yields the following expression:

$$\Delta x(t) = \pi\beta_1 \sin\left(2\pi\tau_1\right) \quad \text{for } 0 < t \le \alpha_{\text{turn}}. \tag{S24}$$

Thus, even with compensation, the maximum peak-to-peak scaling error across the image remains the same as in the uncompensated case, about six times the peak residual.

Supplementary Note 4: Analysis of harmonic model

In this note, we analyze the inverse transfer characteristic of the harmonic model and derive expressions for the coefficients (ξ_i and γ_i). As with the sinusoidal model, an exact inverse function of the harmonic model cannot be obtained; however, the residual peak and peak position can be derived analytically using the method described below.

Rearranging Eq. (18) for τ_i in the forward scan (i = 1) yields the implicit equation as follows:

$$\tau_1 \approx u - 2\xi_1\gamma_1 u - \xi_1\left[\sin\left(\pi\tau_1\right) + \gamma_1\left(\cos\left(\pi\tau_1\right) - 1\right)\right]. \tag{S25}$$

The residual from the ideal linear characteristic of this equation is expressed by:

$$\begin{aligned}\Delta\tau_1 &= \tau_1 - u \\ &= -2\xi_1\gamma_1 u - \xi_1\left[\sin\left(\pi\tau_1\right) + \gamma_1\left(\cos\left(\pi\tau_1\right) - 1\right)\right].\end{aligned} \tag{S26}$$

Substituting Eq. (18) into this equation for u yields:

$$\Delta\tau_1 = -\lambda_1\left\{2\xi_1\gamma_1\tau_1 + \xi_1\left[\sin\left(\pi\tau_1\right) + \gamma_1\left(\cos\left(\pi\tau_1\right) - 1\right)\right]\right\}. \tag{S27}$$

The peak position can be determined from the point where the slope of the function is zero,

$$\frac{\mathrm{d}\Delta\tau_1}{\mathrm{d}\tau_1} = -\lambda_1\left[2\xi_1\gamma_1 + \pi\xi_1\left(\cos\left(\pi u\right) - \gamma_1\sin\left(\pi u\right)\right)\right] = 0, \tag{S28}$$

which gives

$$\tau_1\left(u = u_{\text{peak},1}\right) = \frac{2}{\pi}\tan^{-1}\left(\frac{\sqrt{1+\gamma_1^2 - \left(2\gamma_1/\pi\right)^2} - \gamma_1}{1 - \left(2\gamma_1/\pi\right)}\right). \tag{S29}$$

Next, assuming that the nonlinear term is sufficiently small, the inverse function is obtained using a perturbation method. Expanding the inverse function of Eq. (18) for i = 1 up to the first order yields:

$$\tau_1 \approx u - 2\xi_1\gamma_1 u - \xi_1\left[\sin\left(\pi u\right) + \gamma_1\left(\cos\left(\pi u\right) - 1\right)\right] + O\left(\beta_1^2\right). \tag{S30}$$

The residual of this equation from the ideal linear characteristic is given by:

$$
\begin{aligned}
\Delta\tau_1 &= \tau_1 - u \\
&\approx -2\xi_1\gamma_1 u - \xi_1\left[\sin\left(\pi u\right) + \gamma_1\left(\cos\left(\pi u\right) - 1\right)\right] + O\left(\beta_1^2\right).
\end{aligned}
\tag{S31}
$$

The peak position can be determined from the point where the slope of the function is zero,

$$
\frac{\mathrm{d}\Delta\tau_1}{\mathrm{d}u} = -\alpha_{\text{turn}}\left[2\xi_1\gamma_1 + \pi\xi_1\left(\cos\left(\pi u\right) - \gamma_1\sin\left(\pi u\right)\right)\right] = 0. \tag{S32}
$$

Solving this equation yields a result equivalent to Eq. (S29), and thus the following relation holds.

$$
u_{\text{peak},1}^{(0)} = \tau_1\left(u = u_{\text{peak},1}\right). \tag{S33}
$$

The peak position $u_{\text{peak},1}^{(0)}$ represents $u_{\text{peak},1}$ in the limit as $\beta_1 \to 0$, and its expression coincides with that of τ at the peak position that holds for an arbitrary β_1.

By substituting Eq. (S33) into Eq. (S26), the residual at the peak is obtained as follows:

$$
\Delta\tau_1(u = u_{\text{peak},1}) = -2\xi_1\gamma_1 u_{\text{peak},1}^{(0)} - \xi_1\left\{\sin\left(\pi u_{\text{peak},1}^{(0)}\right) + \gamma_1\left[\cos\left(\pi u_{\text{peak},1}^{(0)}\right) - 1\right]\right\}. \tag{S34}
$$

As in the sinusoidal model, requiring the peak residual to equal $-\beta$ leads to the following condition:

$$
\Delta\tau_1(u = u_{\text{peak},1}) = -\beta_1. \tag{S35}
$$

Combining these two equations and solving for ξ yields Eq. (20). To directly control the asymmetry parameter γ using u_{peak} as a variable, Eqs. (S29) and (S33) are solved for γ, yielding Eq. (21). Substituting Eqs. (S33) and (S35) into Eq. (S26) yields Eq. (22).

The same expressions are obtained for the backward scan (i = 2) by an analogous calculation. The derivation of these expressions allows the inverse transfer function of Eq. (18) to be directly tuned without explicitly computing it.

Supplementary Note 5: Position dependence of calibration in hysteresis correction

In Section 8, we proposed a method for hysteresis correction using the sinusoidal and harmonic models. In this method, the nonlinear parameter β_i is first adjusted using either model so that the overall scan waveform is linearized as much as possible. Subsequently, a structure with a known size is imaged using the linearized scan waveform, and the piezoelectric coefficient is calibrated so that the measured scale matches the known value. Since this calibration is performed using a structure located at the image center, the distance error is minimized at that position. It is important to perform quantitative distance measurements near the image center, particularly in high-speed imaging, where scan waveforms incorporating low-pass characteristics and piezoelectric resonances inevitably cause distortion at the image edges.

On the other hand, at larger scan ranges, hysteresis becomes more significant, while edge distortion is reduced because of the lower scan frequency. Therefore, it is important to evaluate how the overall scaling error depends on the calibration reference position, i.e., the image position used for linear fitting.

For the data shown in Fig. 5, the scaling errors obtained when the fitting was referenced to the left and right edges of the image are shown in Supplementary Fig. 1a–c. Comparison with the scaling errors shown in Fig. 5e,f,j reveals that the shape of the scaling-error curves remains unchanged, while the entire curve shifts vertically depending on the reference position. When the fitting was referenced to the image center, the scaling error became zero near the center, whereas when the fitting was referenced to the left or right edge, the scaling error became zero at the corresponding edge.

To quantitatively evaluate the variation in scaling error over the entire image, the RMS values of the scaling error at all positions were calculated (Supplementary Fig. 1d–f). Because the error changes sign depending on the position, the evaluation was based on the RMS value rather than on a simple integral. The results showed that, for all the cases, the scaling error was minimized when the calibration was referenced to the image center. In all cases, the error increased markedly when the calibration was referenced to the left edge, and increased slightly when it was referenced to the right edge, compared with the center-referenced calibration. These results indicate that calibrating based on a structure located at the image center most effectively suppresses the distance error not only at the image center but over the entire image.

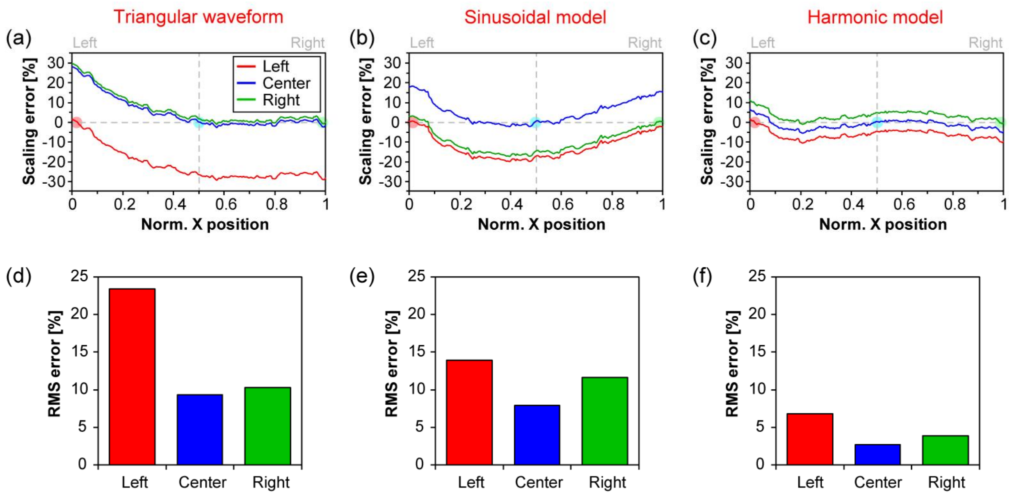

Supplementary Fig. 1. (a–c) Scaling error in scanning as a function of normalized x position when linear fitting was performed at the left edge, center, and right edge of the image for triangular, sinusoidal-model, and harmonic-model input waveforms, respectively. Red, blue, and green circles indicate the reference positions at which the scaling error is zero for the left, center, and right fitting curves, respectively. (d–f) Comparison of the RMS values of the scaling error curves shown in panels a–c for the triangular, sinusoidal-model, and harmonic-model input waveforms, respectively.